University of Nebraska - Lincoln

DigitalCommons@University of Nebraska - Lincoln

2008

Discrete return lidar-based prediction of leaf area index in two conifer forests

Jennifer L.R. Jensen
University of Idaho, jj41@txstate.edu

Karen S. Humes
University of Idaho, khumes@uidaho.edu

Lee A. Vierling
University of Idaho, leev@uidaho.edu

Andrew T. Hudak
Rocky Mountain Research Station, ahudak@fs.fed.us

Follow this and additional works at: https://digitalcommons.unl.edu/usdafsfacpub

🎨 Part of the Forest Biology Commons, Forest Management Commons, Other Forestry and Forest Sciences Commons, and the Plant Sciences Commons

Discrete return lidar-based prediction of leaf area index in two conifer forests

Jennifer L.R. Jensen [a,*], Karen S. Humes [b], Lee A. Vierling [c], Andrew T. Hudak [d]

[a] Environmental Science Program, Department of Geography, McClure Hall 227, P.O. Box 443021, University of Idaho, Moscow, ID 83844, United States
[b] Department of Geography, McClure Hall 203, P.O. Box 443021, University of Idaho, Moscow, ID 83844, United States
[c] Department of Rangeland Ecology and Management, Geospatial Laboratory for Environmental Dynamics, College of Natural Resources, University of Idaho, Moscow, ID 83844-1135, United States
[d] Rocky Mountain Research Station, US Department of Agriculture Forest Service, 1221 South Main Street, Moscow, ID 83843, United States

ARTICLE INFO

ABSTRACT

Leaf area index (LAI) is a key forest structural characteristic that serves as a primary control for exchanges of mass and energy within a vegetated ecosystem. Most previous attempts to estimate LAI from remotely sensed data have relied on empirical relationships between field-measured observations and various spectral vegetation indices (SVIs) derived from optical imagery or the inversion of canopy radiative transfer models. However, as biomass within an ecosystem increases, accurate LAI estimates are difficult to quantify. Here we use lidar data in conjunction with SPOT5-derived spectral vegetation indices (SVIs) to examine the extent to which integration of both lidar and spectral datasets can estimate specific LAI quantities over a broad range of conifer forest stands in the northern Rocky Mountains. Our results show that SPOT5-derived SVIs performed poorly across our study areas, explaining less than 50% of variation in observed LAI, while lidar-only models account for a significant amount of variation across the two study areas located in northern Idaho; the St. Joe Woodlands ($R^2=0.86$; RMSE=0.76) and the Nez Perce Reservation ($R^2=0.69$; RMSE=0.61). Further, we found that LAI models derived from lidar metrics were only incrementally improved with the inclusion of SPOT 5-derived SVIs; increases in R^2 ranged from 0.02–0.04, though model RMSE values decreased for most models (0–11.76% decrease). Significant lidar-only models tended to utilize a common set of predictor variables such as canopy percentile heights and percentile height differences, percent canopy cover metrics, and covariates that described lidar height distributional parameters. All integrated lidar-SPOT 5 models included textural measures of the visible wavelengths (e.g. green and red reflectance). Due to the limited amount of LAI model improvement when adding SPOT 5 metrics to lidar data, we conclude that lidar data alone can provide superior estimates of LAI for our study areas.

© 2008 Elsevier Inc. All rights reserved.

1. Introduction

The foliage component of a forest canopy is the primary surface that controls mass, energy, and gas exchange between photosynthetically active vegetation and the atmosphere (Fournier et al., 2003). A thorough characterization of leaf area index (LAI; the ratio of half of the total needle surface area per unit ground area) can therefore provide valuable information about nutrient cycling, hydrologic forecasting, and biogeochemical processes in a forested ecosystem. As a key vegetation structural characteristic that drives many vegetation functions, LAI is a primary parameter used in ecophysiological and biogeochemical models to describe plant canopies (Chen et al., 1997). For example, process-based models such as BIOMASS (McMurtrie & Landsberg, 1992), FOREST-BGC (Running & Coughlan, 1988) and RHESSys (Band et al., 1991) use LAI as a primary or intermediate variable for forest growth and productivity. Additionally, LAI is often employed as a critical calibration variable for remote

sensing datasets to differentiate vegetation characteristics over a wide range of biomes (Coops et al., 2004). LAI has also been used to characterize forest radiation regimes and the amount of light available to the understory in tropical (e.g. Rich et al., 1993; Vierling & Wessman, 2000) and temperate conifer (e.g. Law et al., 2001a) and deciduous forests (e.g. Ellsworth & Reich, 1993). Given the role of LAI in determining many forest ecosystem processes, several techniques have been developed for rapid LAI estimation.

The most commonly employed methods for estimating LAI across landscapes rely on the relationships between LAI and various manipulations of spectral information from aircraft or satellite-based imagery. A significant amount of research has been dedicated to quantifying the connections between spectral vegetation indices (SVIs) that associate foliar composition in the visible red waveband, which is absorbed by *chlorophyll a* and *b*, and the near-infrared waveband, which is scattered by plant cellular structures. The normalized difference vegetation index (NDVI) (Rouse et al., 1974) and the simple ratio (SR) (Birth & McVey, 1968) are the most frequently used SVIs to estimate LAI for a variety of ecosystem types including coniferous forests (Chen et al., 1997; Curran et al., 1992), grasslands (Friedl et al., 1994) and deciduous forests (Coops et al.,

2004). Recent studies have incorporated more complex vegetation indices by including spectral response from additional wavelengths in an effort to minimize the influences of atmospheric disparities and canopy background noise. For example, a mid-infrared correction proposed by Nemani et al. (1993) to NDVI and SR have been found by White et al. (1997) and Pocewicz et al. (2004) to improve LAI estimates in montane and temperate coniferous forests. Lymburner et al. (2000) developed the specific leaf area vegetation index (SLAVI) to account for mid-infrared sensitivity to varying canopy structure for heterogeneous forest/woodland compositions. Chen et al. (2004) examined the use of the enhanced vegetation index (EVI; Huete et al., 1997) to improve LAI and vegetation cover estimates in a ponderosa pine forest. The reduced simple ratio (RSR) has demonstrated success for estimating LAI in pine and spruce stands (Stenberg et al., 2004) and for a post-fire chronosequence in Siberia (Chen et al., 2005b).

Overall, commonly used SVIs serve as suitable surrogates to approximate LAI for canopies with relatively low LAI (e.g. LAI=3–5) (Chen & Cihlar, 1996; Turner et al., 1999). However, for values above this LAI threshold, many SVIs tend to saturate such that LAI estimates for high biomass forests may be grossly underestimated. For most temperate coniferous forests, the ability to discriminate higher LAI values from optical remote sensing data has been a major challenge.

Lidar data provide an alternative approach for estimating LAI across the landscape. Throughout the past decade, many researchers have reported the utility of lidar data to estimate a suite of forest biophysical characteristics such as canopy height, basal area, crown closure, wood volume, stem density, and biomass (Maclean & Krabill, 1986; Means et al., 2000; Naesset & Bjerknes, 2001; Nelson et al., 1988; Popescu et al., 2003) over a range of forest structural types and regional (Lefsky et al., 2005a) to sub-regional scales (Jensen et al., 2006). More recently, researchers have attempted to relate the three-dimensional structural information captured with lidar data to both direct and indirect estimates of LAI based on various analytical methods. For instance, Magnussen and Boudewyn (1998) found that the proportion of lidar returns corresponding to calculated canopy heights was correlated with the fractional leaf area above canopy-specific height thresholds. Lefsky et al. (1999) explored a three-dimensional (volumetric) analysis of waveform lidar data to estimate leaf area index within a multiple regression framework. Chen et al. (2004) investigated the relationships between trees identified with lidar data tree cover response obtained by a discrete-return system to spectrally-derived vegetation indices and LAI. Riano et al. (2004) and Morsdorf et al. (2006) assessed the capacity of lidar and variable-radius plots to estimate LAI. Lefsky et al. (2005a) developed robust empirical estimates based on waveform lidar and regional LAI measurements for the U.S. Pacific Northwest and Koetz et al. (2006) inverted both actual and simulated 3-D lidar waveform models to estimate LAI and other biophysical parameters within a radiative transfer model.

LAI can be estimated from a variety of remote sensing datasets, warranting the exploration of lidar and multispectral data integration. Lidar/multispectral data integration (also referred to as data fusion or synergy) has been explored for retrieval of other forest characteristics such as canopy height (Hudak et al., 2002; Popescu & Wynne, 2004; Wulder & Seemann, 2003), volume and biomass (Hudak et al., 2006; Popescu et al., 2004), stand density (McCombs et al., 2003), forest productivity (Lefsky et al., 2005b), canopy change detection (Wulder et al., 2007) and characterization of foliage pigments (Blackburn, 2002). However, the potential for spatial and spectral data integration remains significantly unaddressed in terms of quantifying and mapping LAI in moderate to high biomass coniferous forests.

Previous studies of LAI in northern Idaho conifer forests have reported LAI ranging from 0 to 13, with the majority of observations exceeding LAI=4 (Duursma et al., 2003; Pocewicz et al., 2004). In terms of geographic significance, the northern Idaho mountain ranges may represent the region of highest carbon uptake in the Rocky Mountain range, and thus the most substantial carbon sink between the Cascade

Mountains and the Midwestern U.S. (Schimel et al., 2002). Therefore, accurate and reliable estimates of LAI are vital to adequately characterize ecosystem processes and monitor trajectories of change. Currently, operational LAI products from the MODIS sensor and SPOT VEGETATION provide repeat spatial and temporal coverage of biophysical variables used to describe vegetation structure (Baret et al., 2007; Yang et al., 2006), but at a much coarser spatial resolution such that heterogeneity of fine-to-medium scale landscape features is lost.

The specific objectives of our research are to determine 1) the capability of lidar-derived covariates to estimate measured and corrected LAI quantities, 2) the extent to which SPOT 5 spectral data may improve lidar-based LAI estimates, and 3) the applicability of a regional model to quantify LAI in northern Rocky Mountain forests.

2. Materials and methods

2.1. Study areas

Forested regions of northern Idaho exhibit a wide range of stand characteristics representative of conifer forests in the Northern Rocky mountains, and more generally, the western United States. A diverse range of topographic and climatic conditions combined with forest management practices serve to determine species composition and land-use patterns in the Intermountain West. To meet our research objectives, two distinct forested areas were selected to represent the broader range of forest characteristics found throughout the region. Though relatively close in geographic proximity, each study area exhibits contrasting characteristics with regard to topography, species composition, and forest management practices. The St. Joe Woodlands (SJW) study area was selected to represent a cooler, wetter climate regime while the Nez Perce Reservation (NPR) study area characterizes the lower elevation climate of warmer and drier conditions along the western edge of the Rocky Mountains range.

The SJW study area is located between N47°07′–N47°17′ and W115°58′–W116° 22′ and totals approximately 58,684 ha (Fig. 1). In order of dominance by percent basal area conifer species found in the SJW include *Thuja plicata* (THPL), *Abies grandis* (ABGR), *Pseudotsuga menziesii* (PSME), *Larix occidentalis* (LAOC), *Tsuga heterophylla* (TSHE), *Abies lasiocarpa* (ABLA), *Picea engelmanni* (PIEN), *Pinus contorta* (PICO), *Pinus ponderosa* (PIPO), *Pinus monticola* (PIMO). Elevation in the SJW ranges from 658–2000 m with a mean and standard deviation of 1140 m and 244 m respectively. In general, slopes are relatively steep, ranging from 0–50.9° with a mean of 16.9°. Mean annual temperature and total annual precipitation are 8.5 °C and 124.4 cm respectively.

The NPR study area, located between N46°09′–N46°22′ and W116°28′–W116°49′, is subdivided into 5 smaller forested study units totaling approximately 13,350 ha. In order of dominance, conifer species occurring throughout the NPR study area include PSME, PIPO, ABGR, LAOC, PICO, PIEN, and *Taxus brevifolia* (TABR). Elevation ranges from 277–1479 m with a mean and standard deviation of 843 m and 256 m respectively. Slopes range from 0°–48.4°, with a mean of 8.6°. Mean annual temperature and total annual precipitation are 9.8 °C and 64.5 cm respectively.

Overall, both study areas are managed for commercial timber production, though more intensive management is practiced throughout the SJW. Active rotations of large tracts of forest land are common, with a considerable number of selective thinning and clear-cut operations occurring throughout the year. Compared to the SJW, forest stands on the NPR occupy a considerably smaller area and are less intensively managed. Common stand treatments on the NPR include selective thinning and mechanical fuel reduction. Additionally, cattle and goat grazing are also permitted for selected forest stands.

2.2. Field data collection and processing

We established 15 m-radius plots in the SJW (n=46) and across the five separate study units on the NPR (n=50). Both study areas are sites of
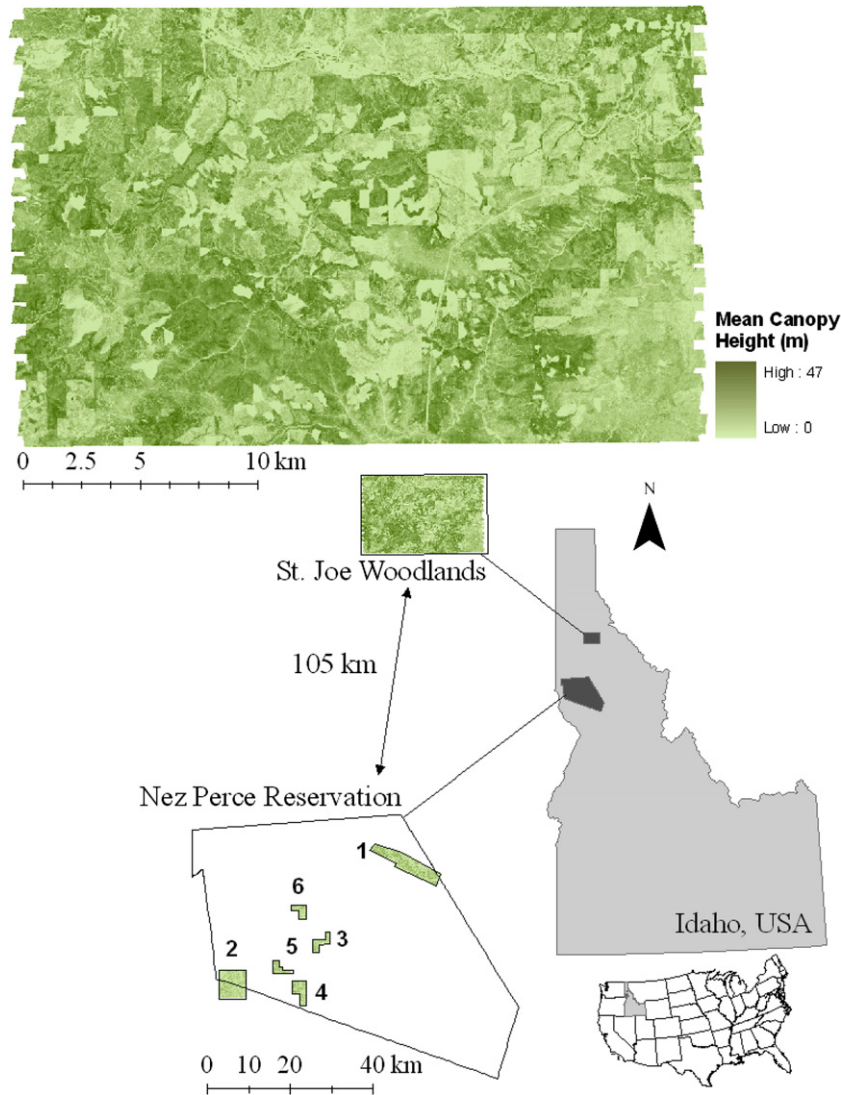
Fig. 1. The SJW and NPR study areas in northern Idaho. The SJW study unit is enlarged (top) to graphically convey landscape heterogeneity expressed as lidar-derived mean canopy height. Minimum canopy height for all NPR units is zero; maximum heights (m) for individual study units are: 1) 23.9, 2) 22.8, 3) 17.6, 4) 17.8, 5) 17.1, and 6) 20.1.

previous studies that utilized lidar data to estimate forest biophysical characteristics. A subset of previously inventoried forest plots were selected for LAI measurements using a stratified random approach to best represent the diversity of species, size, and stand density in proportion to their occurrence. Plots from the SJW were initially established by Hudak et al. (2006) for a lidar-multispectral data integration study to estimate basal area and stem density. Plots from the NPR were previously established by Jensen et al. (2006) to estimate operational forest characteristics from discrete return lidar data. A total of 96 candidate plots were revisited throughout the summer and fall of 2006 and 2007 to collect LAI data for this study. Average distance between plots on the NPR was 729 m and 1.36 km at the SJW.

2.2.1. LAI data collection and processing

LAI sampling protocol followed the design illustrated in Fig. 2. Effective LAI (LAI$_e$) measurements were obtained by employing two LAI-2000 units in remote mode. The LAI-2000 Plant Canopy Analyzer utilizes a fisheye optical sensor comprised of 5 concentric silicon detector rings for a 148° field of view. The instrument simultaneously measures attenuation of diffuse solar radiation as it is transmitted through a forest canopy at multiple view angles (Welles & Norman, 1991). The instrument is fitted with a filter designed to reject wavelengths greater than 490 nm to minimize the contribution of solar radiation transmitted and scattered by foliage.

The first sensor was mounted and leveled on a tripod in a nearby clearing and programmed to automatically log readings of sky condition at 15 second intervals, while the second sensor was used to rove within forest plots to manually collect temporally coincident below canopy readings. To help mitigate the challenge of obtaining above canopy readings in limited clearings and to minimize slope effects, 45-degree view restrictors were affixed to each sensor. Both sets of measurements were obtained with each sensor pointed in the same azimuthal direction. Measurements were obtained during diffuse sky conditions.

Within each plot, three measurements were obtained 1 m on either side of the six LAI sample points, with the sensor held approximately 1.4 m above the ground. In this manner, a total of 36 LAI-2000 instrument readings were obtained per plot. LAI-2000 data were post-processed using the vendor-provided software FV-2000. The first and fifth rings were excluded from LAI calculation due to the sensitivity of Ring 1 to sensor position with respect to crown projection (Law et al., 2001b) and additional contribution of diffuse light in Ring 5 from multiple scattering (Chen et al., 1997).

Since LAI measured by the LAI-2000 instrument assumes a random foliage distribution, it is necessary to correct for clumping and contribution of woody components. Ancillary data used for this analysis included species, DBH, and height information for each tree within each plot. DBH and height were used to calculate species-specific basal area,
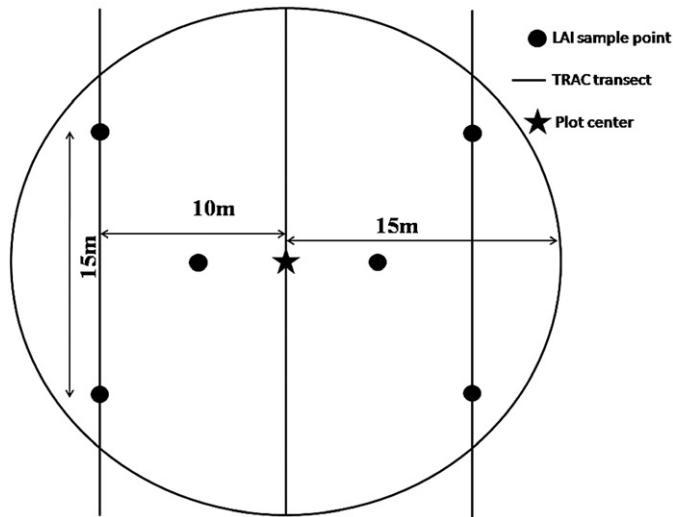
Fig. 2. LAI and TRAC sampling design within a 15 m-radius (0.07 ha) sample plot.

classify dominant species, and species composition. These measures were used to calculate species-specific weighting factors for plot-level γ_E (needle-to-shoot ratio) and α (woody-to-total area ratio) values (Table 1). For this study, a few species are present for which there are no published values for γ_E and α. In such cases, values were inferred from previously published values of structurally and taxonomically similar species. We computed corrected LAI (LAI$_c$) and foliage-only LAI (LAI$_f$) by applying a correction factors developed by Chen et al. (1997):

$$LAI_c = (\Omega_E/\gamma_E)*LAI_e \qquad (1)$$

where Ω_E is foliage clumping at scales larger than the shoot, discussed in detail in Section 2.2.2.

$$LAI_f = (1-\alpha)*LAI_c \qquad (2)$$

2.2.2. TRAC data collection and processing

The Tracing Radiation and Architecture of Canopies (TRAC) instrument developed by Chen and Chilar (1995) is an optical instrument designed to account for the non-randomness of forest canopies by quantifying both canopy gap fraction and gap size, or the physical dimension of gaps in the forest canopy. The canopy gap size distribution is important because it contains information about canopy spatial structure and can be used to quantify foliage clumping effect, or the effect of foliage clumping at scales larger than the shoot, denoted by Ω_E (Chen et al., 1997). Gap size can be derived by recording rapid

(32 Hz) variations in the photosynthetic photon flux density (PPFD) while walking along a transect at a steady pace. A gap size distribution is generated from the spikes caused by high PPFD values (gaps) and low PPFD values (intercepted radiation). Based on the gap size distribution, gaps related to non-randomness are identified and excluded from the total gap fraction using a gap removal method. The clumping effect, Ω_E, is calculated as the difference between measured gap fraction and the gap fraction after non-random gaps have been removed.

TRAC measurements were obtained by walking the three transects established for every plot during clear sky conditions and with solar zenith angle ranging between 30 and 60 degrees. Immediately before or after a set of plot measurements, a reference reading was collected in an open clearing as near the plot as possible. Within the plot, the sensor was carried along each transect at a minimum speed of 1 m per 3 s in the same direction (SW–NE) for each transect. TRAC data were post-processed using the analysis software TRACWin (Version 3.9.0). The three transects obtained for each plot were averaged to represent plot-level Ω_E.

2.3. Lidar data collection and processing

Lidar data were acquired during the summers of 2002 and 2003 for the NPR and SJW respectively. Both data missions employed a Leica ALS40 lidar sensor and similar acquisition parameters (Table 2). Raw lidar data containing the X, Y, and Z coordinates for each return were delivered in ASCII format for individual flightlines and imported into ArcInfo (ESRI, Redlands, CA) to classify ground versus non-ground returns using the Multi Curvature Classification (MCC) method (Evans & Hudak, 2007) to generate digital terrain surface layers. Canopy heights were calculated by subtracting corresponding MCC-generated terrain surfaces from the original (unclassified) lidar datasets. Finally, the calculated canopy height returns were clipped from each dataset to correspond with the field measured sample plots.

Calculated canopy heights were extracted for individual plots and processed to produce standard lidar regression covariates including mean, variance, coefficient of variation, skewness, kurtosis, and the 25th, 50th, 75th and 95th percentile values of all returns and returns greater than 1.4 m. Additional metrics summarizing the difference in percentile heights were computed to characterize where biomass was distributed within the canopy. Lastly, metrics corresponding to the percentage of returns within specified height intervals were computed based on height thresholds equivalent to standard tree-size diameter breaks. Refer to Table 3 for a summary of lidar-derived metrics.

2.4. SPOT 5 data acquisition and processing

Two SPOT 5 Level 1B images were acquired over the NPR on June 28, 2003 and a single SPOT 5 Level 1A image was acquired for the SJW August 20, 2006. SPOT 5 data are 10 m spatial resolution in the green (500–590 nm), red (610–680 nm), and near-infrared (780–890 nm) portion of the electromagnetic spectrum and 20 m spatial resolution

Table 1
Species specific needle-to-shoot ratio (γ_E) and woody-to-total area ratio (α) used to correct LAI$_e$

Species	γ_E	α	Source
Abies grandis	2.35	0.12–0.17[a]	(Gower et al., 1999; Roberts et al., 2004)
Abies lasiocarpa	2.35	0.12–0.17[a]	(Gower & Norman, 1991; Roberts et al., 2004)
Larix occidentalis[b]	1.49	0.12–0.17[a]	(Gower & Norman, 1991)
Picea engelmannii[b]	1.57	0.12–0.17[a]	(Chen et al., 2006; Gower et al., 1999)
Pinus contorta[b]	2.08	0.28	Hall et al. (2003)
Pinus monticola	3.4	0.11–0.34[a]	(Frazer et al., 2000; Gower et al., 1999)
Pinus ponderosa	1.25	0.27	Law et al. (2001a,b)
Pseudotsuga menziesii	1.77	0.08	Gower et al. (1999)
Thuja plicata	1.01	0.15	Roberts et al. (2004)
Tsuga heterophylla	1.38	0.15[c]	Frazer et al. (2000)
Tsuga mertensiana[b]	1.38	0.15[c]	Frazer et al. (2000)

[a] Multiple reported values; average used for analysis.
[b] Correction based on similar species.
[c] Based on species similarity.

Table 2
Lidar acquisition parameters

Acquisition parameter	SJW	NPR
Date acquired	2003	2002
Sensor	Leica ALS40	Leica ALS40
Wavelength (nm)	1064	1064
Flight height (m)*	2438	1828
Footprint diameter (cm)	30	60
Post-spacing (m)	1.95	2.0
Scan/Pulse rates (Hz/kHz)	17.1/20.0	17.1/20.0
Scan angle (°)	+/−20**	+/−12.5
Average swath width (m)	904	810.77
Average point density (m²)	0.26	0.36

* Above mean terrain.
** Scan angles >15° were discarded (after Hudak et al., 2006).

Table 3
Lidar-derived model covariates

Metric classification	Threshold (m)	Label
Canopy height metrics		
Canopy percentiles	All points	CAN$_{25ile}$, CAN$_{50ile}$, CAN$_{75ile}$, CAN$_{95ile}$, MAX_HEIGHT (CAN$_{100ile}$).
Upper-story percentiles	>1.37	LUPP$_{25ile}$, LUPP$_{50ile}$, LUPP$_{75ile}$, LUPP$_{95ile}$
Fixed percentile differences	All points and >1.37	DIFF25, DIFF50, DIFF75, DIFF95 — Difference between upper-story percentiles and corresponding canopy percentiles
Variable percentile differences	All points and >1.37	L95_C25, L75_C25, L50_C25, ...etc. Difference between upper-story percentiles and various canopy percentiles
Canopy cover metrics		
% Understory cover	0.03–1.37	LUSC
% Canopy cover 1	1.38–10.67	LCCO1
% Canopy cover 2	10.68–18.29	LCCO2
% Canopy cover 3	18.30–28.96	LCCO3
% Canopy cover 4	>28.96	LCCO4
% Canopy cover 123	>1.38–28.96	LCCO123
% Canopy cover above	>1.37	LCCOABOVE
Total % canopy cover	>0.03	LCCOTOTAL
Height distribution metrics		
Mean	All points	LH$_{Mean}$
Variance	All points	LH$_{Var}$
Coefficient of variation	All points	LH$_{Coef}$
Kurtosis	All points	LH$_{Kurt}$
Upper-story Mean	>1.37	LUPP$_{Mean}$
Upper-story variance	>1.37	LUPP$_{Var}$
Upper-story coefficient of variation	>1.37	LUPP$_{Coef}$
Upper-story kurtosis	>1.37	LUPP$_{Kurt}$

Values are calculated per plot based on calculated vegetation heights.

in the shortwave infrared (1580–1750 nm). All images were acquired with scan angles <5° and <10% cloud cover. Images were orthorectified to corresponding digital orthoimagery quarter quadrangles (DOQQs) and re-projected to the UTM (Zone 11) coordinate system defined for the lidar acquisition. Raw image data were radiometrically corrected and converted to exoatmospheric reflectance to reduce between-scene variability owing to variation in solar irradiance at the time of acquisition. The 10 m spatial resolution of SPOT imagery

Table 4
SPOT-derived model covariates

Metric	Equation	Reference
BAND_MEAN	Average spectral response within a plot (e.g. GREEN, RED, NIR, MIR)	
BAND_STDEV	Standard deviation of spectral responses within a plot (e.g. GREEN, RED, NIR, MIR)	
Normalized Difference Vegetation Index (NDVI)	$NDVI = \frac{\rho nir - \rho red}{\rho nir + \rho red}$	Rouse et al. (1974)
Mid-Infrared Corrected NDVI (NDVIc)	$NDVIc = \frac{\rho nir - \rho red}{\rho nir + \rho red} \times \left[1 - \frac{(\rho MIR - \rho MIRmin)}{(\rho MIRmax + \rho MIRmin)} \right]$	Nemani et al. (1993)
Simple Ratio (SR)	$SR = \frac{\rho nir}{\rho red}$	Birth and McVey (1968)
Reduced Simple Ratio (RSR)	$RSR = \frac{\rho nir}{\rho red} \times \left[1 - \frac{(\rho SWIR - \rho SWIRmin)}{(\rho SWIRmax + \rho SWIRmin)} \right]$	Chen et al. (2002)
Mid-Infrared Corrected SR (SRc)	$SRc = \frac{\rho nir}{\rho red} \times \left[1 - \frac{(\rho MIR - \rho MIRmin)}{(\rho SWIRmax - \rho SWIRmin)} \right]$	Brown et al. (2000)
Green–Red Vegetation Index (GRVI)	$GRVI = \frac{\rho green - \rho red}{\rho green + \rho red}$	Tucker et al. (1979)

Values based on exo-atmospheric reflectance.

Table 5
Field-obtained effective LAI (LAI$_e$) and corrected values calculated from plot- and species-specific correction factors

Dataset		LAI$_e$	LAI$_c$	LAI$_F$
SJW	Mean(S.D.)	3.44(1.47)	6.37(2.51)	5.41(2.21)
n=46	Range	0.70–6.1	1.1–10.9	1.0–9.2
NPR	Mean(S.D.)	1.89(1.05)	3.92(2.35)	3.35(2.13)
n=50	Range	0.40–4.8	0.40–10.4	0.40–9.6
COMBINED	Mean(S.D.)	2.63(1.48)	5.01(2.72)	4.26(2.40)
n=96	Range	0.40–6.1	0.40–10.9	0.40–9.6

facilitated calculation and inclusion of textural measures for LAI models, whereas this would not be possible with at the same level of detail with coarser-resolution imagery such as Landsat ETM+. Wulder et al. (1998) suggested that textural information could improve characterization of forest structure, particularly as the strength of standard SVI-LAI relationships weakens.

A series of SVIs were calculated for each image as well as average reflectance and texture information for each band. The ZONALSTATS tool in ArcINFO was used to extract plot-level SVI and reflectance average values of all pixels that intersected the plot area. The standard deviation (BAND_STDEV) of individual band reflectance was taken as a direct statistic based on the same plot-pixel intersection method. On average, information from seven SPOT 5 10 m pixels were used for each SPOT 5 (hereto referred to as SPOT) covariate. Refer to Table 4 for a list of SPOT model covariates calculated for analysis.
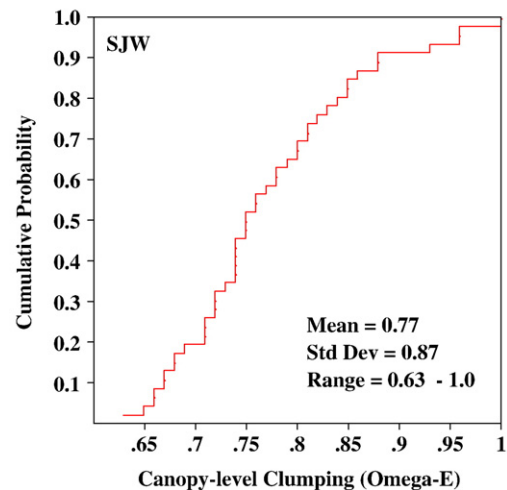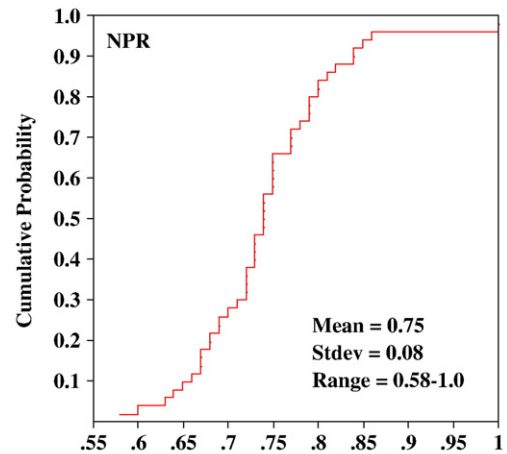

Mean = 0.75
Stdev = 0.08
Range = 0.58-1.0

Mean = 0.77
Std Dev = 0.87
Range = 0.63 - 1.0

Fig. 3. Cumulative distribution functions and univariate statistics of canopy-level clumping index values, Ω_E by study area.

2.5. Statistical analysis

The NPR and SJW were analyzed separately and as a combined dataset within a multiple regression framework. The statistical analysis software (SAS) package (SAS Institute, Cary N.C.) was employed to model leaf area index quantities (i.e. LAI_e, LAI_c, and LAI_f) using the best subsets regression procedure available in PROC REG. Several criteria were used to examine potential models including R^2 and adjusted R^2, root mean square error (RSME) and AICc (Suguira, 1978). Once candidate models were identified, a more rigorous selection approach was applied, including individual covariate significance, (Type III error t tests, $\alpha = 0.05$), absence of multicollinearity (i.e. tolerance>0.1, Neter et al., 1985), and residual homoscedasticity. All criteria had to be satisfied for final model consideration. The Predicted Residual Sum of Squares (PRESS) statistic (Allen, 1971) was used to assess the prediction error of candidate models. The PRESS statistic is effectively a leave-one-out cross validation approach, where the model is re-parameterized with $n-1$ observations, and the $n-1$ model is used to predict the excluded response. Final models were those that exhibited a combination of the lowest AICc, smallest changes in R^2 to adjusted R^2 and the lowest full-dataset RMSE to PRESS RMSE ratio, while still satisfying individual covariate criteria. These model selection criteria were applied in an effort to develop robust models and prevent model overfit from inclusion of excessive or redundant covariate terms. AICc is an information criterion that addresses model dimensionality, providing a relative comparison of covariate multicollinearity effects. Exclusion of redundant covariates was also addressed by examination of individual tolerance values. Model validity in multivariate linear regression relies partly on the ratio of the number of observations to the number of model covariates. Since adjusted R^2 is more conservative than R^2, we sought models that exhibited small changes between the two statistics. Lidar models were

selected first based on the criteria outlined above. After the lidar model selection, SPOT band data and indices were added to the analysis. The best subset method was still used, however only those covariates from the selected lidar model were included in the analysis with SPOT data. Resultant models were subject to the same criteria used to select lidar-only models. In addition, to determine if the selected SPOT variables added significant predictive value to the final models, a subset of regression coefficients were tested using the complete (lidar-SPOT) and reduced (lidar-only) models.

3. Results

Exploratory data analysis indicated that LAI quantities were not normally distributed; thus, response data were transformed to satisfy the normality assumption for linear regression. A natural log transformation was used for the SJW and a square root transformation for the NPR. The combined dataset used the square root and natural log transformation for LAI_e and corrected LAI quantities, respectively. Different transformations were required for the combined dataset because a single transformation did not result in a normal distribution for all LAI quantities. LAI estimates were back-transformed using the appropriate algorithm.

Results for each study area and as a combined dataset (denoted 'COMBINED') are summarized for specific LAI quantities and the specific regression-based analysis (i.e. lidar-only, SPOT-only, and lidar-SPOT models).

3.1. Effective LAI, TRAC measurements, and corrected LAI quantities

LAI_e for all plots sampled from both study areas (i.e. COMBINED), ranged from 0.40–6.1 (mean 2.63, S.D. 1.48). Overall, LAI_e measured on the NPR had a smaller range and mean value than plots measured in the SJW; mean LAI_e of plots on the SJW was 3.44, nearly twice that of the NPR (1.89). When LAI_e was corrected for clumping, the range of LAI_c values increased for both study areas. Table 5 provides univariate statistics for all LAI quantities.

Table 6
Results of lidar-only regression analysis of specific LAI quantities

Dataset	Variable	Lidar model	R^2	Adj. R^2	RSME
SJW $n=46$	(ln)LAI	$1.2271 - 0.1234$ (LHKURT) -0.0470 (LUPP25ILE) $+0.0787$(MAX_HEIGHT) $- 0.1079$(L95_C25)	0.8612	0.8476	0.76
	(ln)LAI_c	$1.2491 - 0.1536$(LHKURT) $+.6363$ (LUPPCOEF) $+.0540$(MAX_HEIGHT) $- 0.1052$(L95_C25)	0.7430	0.7179	1.8
	(ln)LAI_f	$1.0941 - 0.1587$(LHKURT) $+.6728$ (LUPPCOEF) $+0514$(MAX_HEIGHT) $- 0.1028$(L95_C25)	0.7098	0.6815	1.7
NPR $n=50$	(sqrt) LAI	$1.2963 - 1.4051$(LCCO3) $+0.0266$ (MAX_HEIGHT) $+0.7982$ (LCCOABOVE) -0.0154(L25_C25) $- 0.0378$(L95_C50) $+0.0276$(L50_C50)	0.8612	0.8476	0.76
	(sqrt) LAI_c	$1.5249 - 3.0071$(LCCO3) $+1.4242$ (LCCOABOVE) $+0.0060$(LUPPVAR) $+ 0.0360$(MAX_HEIGHT) -0.0747 (L95_C25) $+0.0465$(L50_C50)	0.7430	0.7179	1.8
	(sqrt) LAI_f	$1.3938 - 2.8703$(LCCO3) $+1.3430$ (LCCOABOVE) $+0.0055$(LUPPVAR) $+ 0.0360$(MAX_HEIGHT) -0.0711 (L95_C25) $+0.0449$(L50_C50)	0.7098	0.6815	1.7
COMBINED $n=96$	(sqrt) LAI	$1.8562 + 0.7436$ (LCCOABOVE) $- 0.6955$ (LUPPCOEF) -0.0314 (LUPP25ILE) $+0.0355$ (MAX_HEIGHT) $- 0.0396$ (L95_C25)	0.6971	0.6548	0.61
	(ln)LAI_c	$2.3053 - 0.3057$(LHSKEW) $+0.0065$ (LUPPVAR) -0.0563(LUPP75ILE) $+ 0.0404$(MAX_HEIGHT) -0.0387 (L95_C25)	0.7230	0.6843	1.3
	(ln)LAI_f	$2.1316 - 0.2919$ (LHSKEW) $+0.0060$ (LUPPVAR) -0.0548 (LUPP75ILE) $+ 0.0401$ (MAX_HEIGHT) -0.0370 (L95_C25)	0.7191	0.6799	1.1

All model covariates significant for $p \leq 0.05$.

Table 7
Results of SPOT-only regression analysis of specific LAI quantities

Dataset	Variable	SPOT Covariate	R^2	RSME
SJW $n=46$	(ln) LAI_e	$NDVI_c$	0.4918	2.7
	(ln) LAI_c	$NDVI_c$	0.3341	2.4
	(ln) LAI_f	$NDVI_c$	0.2972	2.1
NPR $n=50$	(sqrt) LAI_e	RSR	0.2747	1.5
	(sqrt) LAI_c	RED_MEAN	0.2740	2.0
	(sqrt) LAI_f	RED_MEAN	0.2653	1.8
COMBINED $n=96$	(sqrt) LAI_e	MIR_MEAN	0.4631	1.5
	(ln) LAI_c	MIR_MEAN	0.3617	3.2
	(ln) LAI_f	MIR_MEAN	0.3459	2.9

* $p < 0.0001$.

Table 8
Lidar-SPOT model results for specific LAI quantities

Dataset		Lidar-only R^{2*}	Lidar-SPOT R^{2*}	Lidar-only RMSE	Lidar-SPOT RSME	F-stat ($Pr>F$) full vs. reduced model
SJW $n=46$	LAI_e	0.8612	0.8821	0.76	0.71	7.09 ($p=0.0111$)
	LAI_c	0.7430	0.7806	1.8	1.7	6.85 ($p=0.0124$)
	LAI_f	0.7098	0.7513	1.7	1.5	6.68 ($p=0.0135$)
NPR $n=50$	LAI_e	0.6971	0.7246	0.61	0.58	4.13 ($p=0.0231$)
	LAI_c	0.7230	No Imp.	1.3	N/A	
	LAI_f	0.7191	No Imp.	1.1	N/A	
COMBINED $n=96$	LAI_e	0.7513	0.7882	0.75	0.69	7.66 ($p=0.0009$)
	LAI_c	0.6315	0.6494	1.8	1.7	4.53 ($p=0.0360$)
	LAI_f	0.5964	0.6179	1.6	1.6	5.00 ($p=0.0278$)

* $p < 0.0001$.

The cumulative distribution functions in Fig. 3 illustrate the proportion of plots at or above a specified canopy clumping value, Ω_E. A larger value typically indicates less canopy-level clumping and thus a more random distribution of foliage. However, larger Ω_E values for our study appear to be indicative of a more open canopy structure, whereas smaller Ω_E values appear to correspond with a more closed overstory canopy. Plot-averaged TRAC measurements ranged from 0.58 to 1 and 0.63 to 1 on the NPR and SJW, respectively, with similar mean, median, and standard deviations among the study areas.

3.2. Lidar-only LAI estimates

Lidar model covariates performed well, with all models significant at $p < 0.0001$. In terms of effective LAI, the lidar-only model for the SJW was the best, explaining 86% variation in measured values. Differences in R^2 between the SJW and NPR datasets were non-negligible. Given a similar number of measured plots and within-area species variability, the SJW LAI_e lidar model accounted for 15% more variation than the NPR equivalent. However, RMSEs among selected lidar-only models were lower for the NPR. As anticipated, the COMBINED model performance was intermediate to the performance of models from the individual study areas, explaining 75% of variation in observed LAI.

Both R^2 and RMSE decreased considerably between LAI_e and LAI_c/LAI_f in both the SJW and COMBINED datasets. The R^2 increased for these quantities on the NPR, while RMSE exhibits a similar trend to that of the other statistics. For all cases, RMSE increased by a factor of two for corrected LAI quantities when compared to LAI_e errors. Refer to Table 6 for a summary of lidar-only model covariates and analysis results.
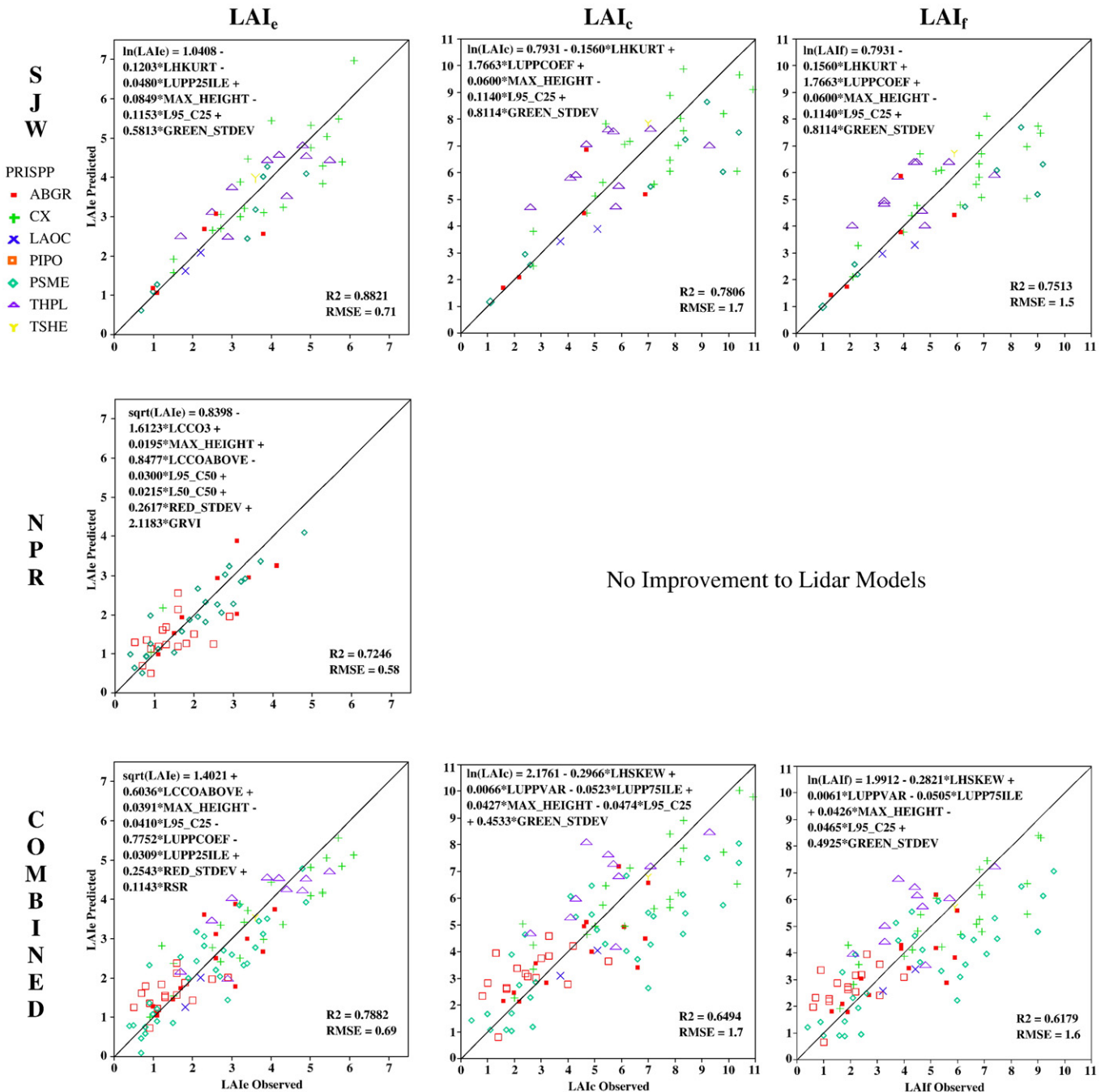

Fig. 4. Scatterplots of Lidar-SPOT integration to estimate specific LAI quantities for individual datasets. Line indicates 1:1 relationship.

3.3. SPOT-only LAI estimates

Regression of individual SPOT model covariates resulted in poor model performance overall. Table 7 summarizes results of SPOT-only regressions for specific LAI quantities. Best model fits were obtained from selection of the mid-infrared corrected NDVI (NDVI$_c$) for the SJW and RSR and average visible red reflectance at the NPR. For the COMBINED dataset, average mid-infrared (MIR_MEAN) reflectance produced the best model fits. Although all SPOT models were statistically significant ($p < 0.0001$), R^2 values were very low overall; the maximum R^2 obtained from optically-derived SPOT imagery was 0.4918 ($p < 0.0001$) for SJW LAI$_e$.

3.4. Lidar-SPOT integrated LAI estimates

Individual SPOT band data and SVIs described in Table 4 were added to the regressions once a suitable lidar-only model was selected. Overall, addition of SPOT data increased the overall R^2 and decreased RMSE for most models, although the improvements for all cases were slight. For instance, the SJW integrated LAI model improved R^2 by roughly 2% and decreased RMSE by 0.05. No improvement was noted for LAI$_c$ or LAI$_f$ on the NPR with the addition of SPOT data.

For all cases except NPR and COMBINED LAI, a single SPOT covariate was added to the model while still satisfying model suitability criteria (e.g. individual variable significance < 0.05 and tolerance > 0.1). In the case of integrated LAI$_e$ estimates for the NPR and COMBINED datasets, two SPOT covariates were added to each model (a single lidar covariate was removed). For all SJW models and COMBINED LAI$_c$ and LAI$_f$, the only significant SPOT variable added to the lidar models was the standard deviation of the green band (GREEN_STDEV). The NPR LAI$_e$ model showed slight improvement by adding mean red reflectance and GRVI as covariates. The COMBINED LAI model also showed slight improvement by including the mean red spectral response and RSR for LAI. Table 8 summarizes the differences between lidar-only and lidar-SPOT integrated datasets as well as results for complete and reduced model tests. Fig. 4 provides scatterplots of the integrated models and corresponding model equations.

4. Discussion

4.1. Regression analysis

Lidar-derived covariates explained the largest proportion of variation in LAI and corrected quantities among the three datasets used in this analysis. Although existing methods to estimate LAI often rely on a single optically-derived SVI, the relationships are often asymptotic and can result in unreliable estimates for moderate to high biomass forests. The number of lidar covariates selected for each model was a balance between parsimony and relevance, or the explanatory value of individual model terms. Although covariates included in the lidar-only models differed for specific quantities and among study areas, the types of metrics combined in each model were similar. For example, all models (with the exception of lidar-only and integrated LAI$_e$ models on the NPR) included a minimum of one covariate from the each of following three categories: 1) canopy height metrics (e.g. LUPP25ile), 2) height distribution metrics (e.g. LHSKEW), and 3) canopy cover metrics (e.g. LCCOABOVE).

Most models incorporated lidar covariates associated with upperstory metrics.

The lidar covariate, MAX_HEIGHT, is present in every LAI model. Its inclusion follows a line of logic: increases in canopy height should correlate to increases in LAI, however as an independent covariate, MAX_HEIGHT does not significantly correlate with LAI quantities. Inclusion of upper-canopy related metrics is sensible: upperstory

metrics were computed from lidar-derived heights at or above a threshold of 1.4 m (4.5 ft), which corresponds to the standard height at which DBH is measured for most forest survey and inventory applications. Additionally, for most forest types, the bulk of vegetation biomass is located above this height threshold. By implementing this minimum height threshold for upperstory metrics, within-plot lidar returns and the corresponding metrics are limited to the vertical space in which the greatest amount of foliage is distributed. Similarly, LAI observations collected in the field were collected at the same height (1.4 m).

In terms of vertical foliage distribution, a similar line of logic was followed via the calculation of differences in percentile heights (e.g. LUPP95ile–CAN25ile). We presumed that from multiple-return lidar data, the difference in corresponding percentile heights would yield an indication of the vertical distribution of vegetation biomass within each plot. Although we used a combinatorial approach of percentile height differences, the approach can be likened to an index derived by Lefsky et al. (1999) in which canopy height range was computed from an array of lidar waveforms. Since discrete-return lidar only samples the landscape, we tried several combinations to "maximum-minimum" height metrics. As with the MAX_HEIGHT metric, L95_C25 is included in every LAI model.

Percent cover metrics (e.g. LCCO3; LCCOAbove) included in the selected LAI models also correspond to upperstory lidar metrics, again where we expect the greatest density of foliage biomass. Height-threshold subclasses associated with percent height metrics correspond to standard tree-size diameter breaks derived from tree height and diameter regressions developed by the Nez Perce Tribal Forestry Department. Though initially developed to categorize trees for saw-log volume divisions, the height thresholds also capture the height–diameter relationships related to age classes, where larger saw-log volumes are characteristic of more mature stands. Similar, temporally-extensive forest inventory data were not available for the SJW. As such, height-diameter class breaks and percent cover lidar-height thresholds were not modeled, though we acknowledge that differences in species composition, silvicultural prescription, and site quality will influence tree height and diameter relationships. In that regard, final lidar-only models did not include any of the percent cover metrics, however, candidate models from the best subset procedure did occasionally incorporate LCCOAbove.

Lidar models for the SJW required fewer covariates (4) to estimate a larger range of LAI$_e$ than the NPR, which required 6 terms even though the variance on the NPR is half that of the SJW. This may be due in part to the foliage density and leaf orientation of most-dominant species present in each study area. Though species composition is mixed for both study areas, THPL, which has a relatively flat, leaf-like structure, is dominant at the SJW, as opposed to PIPO and PSME, the two most dominant species on the NPR. Leaf geometry and crown structural properties of THPL may provide a larger, more uniform reflective surface as opposed to species that exhibit increase foliage clumping. The leaf-like structure of THPL may result in less scattering of the lidar pulse, thus reflecting a sufficient amount of energy to trigger a first return higher in the canopy.

A second consideration with regard to lidar covariate selection between study areas is the structural characteristics of individual species. For example, many species present on the SJW, and to a lesser extent the NPR, have a relatively uniform crown shape that homogeneously extends from the top of the canopy well toward the understory. Conversely, many of the plots on the NPR are comprised of PIPO, a shade-intolerant species that tends to self-prune, or shed lower branch whorls as it matures. This often results in a tree that may be 30 m tall, but have only 7 m of live foliage. In terms of LAI estimation, percentile heights may be relatively large but LAI is unexpectedly low, whereas for a PSME- or THPL-dominated stand with similar stem density, LAI would be much larger. It should be noted, however, that PIPO is not the only species to exhibit such

physical attributes and that other species may display similar crown characteristics due to other factors such as stocking density. However, in general, the frequency of PIPO occurrence and observations of anomalous crown characteristics are more prevalent on the NPR.

Lidar-only and integrated models to estimate LAI_c and LAI_f for the SJW and COMBINED datasets did not perform as well as the model for LAI_e (e.g. lower R^2 and higher residual errors). This is likely due to the increased variance resulting from applying plot- and species-specific correction factors to LAI_e to account for clumping. For instance, the variance of LAI_c increased 190% compared to LAI_e for the SJW. With a larger range of values to estimate, lower R^2 values and higher residual errors should be expected. However this is not the case for the NPR, where LAI_c and LAI_f estimates were improved despite a near 400% increase in variance between LAI_e and LAI_c. We believe this is due to the near-homogeneity of species-specific correction factors applied to plots on the NPR versus the SJW.

The overall correction factor applied to LAI_e to correct for clumping is more strongly influenced by the species-specific γ_E than plot-measured Ω_E. Mean foliage clumping γ_E values for the SJW were lower due in large part to the leaf-like properties of THPL ($\gamma_E = 1.014$), the most dominant species in the study area. Increases in LAI when $\gamma_E = 1.014$ are small when compared to other species such as PSME ($\gamma_E = 1.77$) or ABGR ($\gamma_E = 2.35$). We expect that an increase in LAI would be accompanied by a corresponding increase in canopy height or percent cover. However, on the SJW, clumping corrections did not follow such logic. Corrections applied to THPL-dominated plots did not significantly increase the LAI in the same manner as AGBR- or PSME-dominated corrections. Plots on the NPR were commonly characterized by a single dominant species. As such apply correction factors to LAI_e for clumping on the NPR simply applied a uniform scalar to 80% of the plots in the study area.

Lidar data can provide valuable canopy information such as height and percent cover but, as anticipated, did not distinguish relative changes in foliage-level geometry (i.e. needle-to-shoot ratios) that contribute to the determination of individual clumping factors. When clumping is accounted for by basal area weighted correction factors over mixed-species stands, it results in an increase in observed LAI that is not readily detected by the lidar system.

4.2. Addition of SPOT covariates

Integrating SPOT-derived SVIs only slightly improved the LAI estimates relative to those obtained via lidar metrics alone. Given that the red and near infrared bands, and at times, the mid-infrared are the most common wavelengths used to characterize vegetation amount, health, and productivity, we anticipated that their integration with lidar would serve to significantly increase the model capacity to estimate LAI. However, only the LAI_e models for the NPR and the COMBINED dataset utilized information related to red reflectance.

Only spectral information calculated with bands from the visible portion of the electromagnetic spectrum (EMS) were selected as covariates in the integrated lidar-SPOT models. GREEN_STDEV, representative of texture, was the most prevalent SPOT covariate included in integrated models. Green leaf/needle spectral response is characterized by high absorptance of photosynthetically active radiation in the blue and red spectra and peak reflectance in the green spectra. Inclusion of green spectral response to estimate LAI, while not as common as red or NIR reflectance, is not unprecedented. For instance, Gitelson et al. (2004) developed a SVI that incorporated green reflectance because it was found to remain sensitive to changes in LAI for maize canopies (particularly LAI > 3), and Walthall et al. (2004) applied Gitelson et al.'s (2004) index to estimate LAI of corn and soybean canopies. Falkowski et al. (2005) found that information contained in the visible portion of the EMS (e.g. green and red

wavelengths; GRVI) had increased predictive value compared to NDVI and SR for estimating canopy closure of mixed conifer stands in northern Idaho. Cosmopoulos and King (2004) included green and red textural covariates derived from high resolution digital camera imagery to improve prediction of a forest structural index developed by Olthof and King (2000) in a mixed boreal forest in northern Ontario, Canada. Image texture information is not limited to visible information contained in visible wavelengths. Wulder et al. (1998), in a study of LAI for mixed-wood stand in southeast New Brunswick, Canada, reported maximum improvement to R^2 from inclusion of textural measures derived from both red and near infrared wavelengths obtained from the compact airborne spectrographic imager (CASI).

4.3. Consideration of error sources

Several sources of error are considered within the scope of interpreting results of our study. First, there are temporal discrepancies between the lidar, SPOT, and LAI data acquisitions. Maximum temporal differences in lidar acquisition versus LAI measurements range from 4 to 5 years for the SJW and NPR, respectively. Furthermore, SPOT data for the NPR were collected to correspond with the study area's lidar acquisition; however this was early in the summer of 2002, while LAI measurements for the area were collected in the late summer and/or fall of 2006 and 2007. The SJW SPOT 5 image was collected in August 2006 to correspond with the field sampling but 3 years after the lidar acquisition. Issues corresponding to vegetation phenology, particularly for understory vegetation and deciduous components, may have influenced the capacity of the SPOT 5 data to more accurately quantify LAI. We mitigated some of these discrepancies by only sampling plots that were not treated (e.g. cleared, thinned, mechanical fuel reduction, etc.) between lidar and field data acquisitions. Very young stands were also excluded from our analysis based on the rationale that young stands would grow at a more rapid rate, and thus exhibit greater differences than more mature stands. Despite the temporal inconsistencies, models were able to account for a significant proportion of variation in LAI for both study areas and the region as a whole because changes in LAI of conifer stands, excluding disturbance, are gradual and typically occur over the course of several growing seasons. This is consistent with the findings of Grier and Running (1977) who, in a study of leaf area of mature conifer forests in the Pacific Northwest, cited previous research to state that "leaf area of forest communities reaches a more of less steady state early in succession."

Additional sources of error may be attributed to data acquisition parameters and processing techniques. For instance, relationships among biophysical characteristics and satellite imagery can be influenced by solar elevation, viewing geometry, soil background and moisture concentrations (Jacquemoud et al., 1995) and atmospheric corrections (Running et al., 1986). Errors in LAI sampling strategy and measurement theory may also influence empirical relationships. Topographic characteristics, consistency between reference (i.e. above-canopy) and under-canopy readings, and canopy architecture can contribute to uncertainty. While reasonable efforts were taken to lessen potential error sources some situations are seemingly unavoidable. For instance, since PIPO exist in relatively open canopy systems, the LAI-2000 sensor is more likely to underestimate LAI in mature dominant and co-dominant PIPO stands due to disproportionate weighting of canopy gaps observed on one side of the sensor compared to relatively few contacts measured from a single or few PIPOs within a plot.

Lastly, the suitability and reliability of ordinary least squares regression, whilst the most commonly employed empirical estimation tool to relate remote-sensing data to field observations has been questioned due to ambiguity in variable specification and measurement error of predictor variables (Curran & Hay, 1986). Several recent

studies (Cohen et al., 2003; Fernandes & Leblanc, 2005; Lefsky et al., 2005a; Pocewicz et al., 2007) have examined alternative empirical regression procedures to estimate forest structural characteristics in consideration of such issues. Finally, alternative methods to regression have also been evaluated. For example, Magnussen and Boudewyn (1998) found that plot-level LAI could be described as a function of the vertical distribution of lidar pulse returns within a plot. In general, analysis of foliage height profiles to characterize LAI and other canopy structure characteristics is a topic of interest (Coops et al., 2007; Lefsky et al., 1999; Lovell et al., 2003) as is relating lidar data to canopy gap fraction theory for LAI estimation using both aircraft (Hopkinson & Chasmer, 2007) and ground-based lidar (Clawges et al., 2007; Danson et al., 2007).

5. Conclusion

The two selected study areas represent a diverse assemblage of ecoregional characteristics, climatic conditions, and anthropogenic influences including management ideology and implementation. Such factors control the type, density, and location of vegetation both within an individual stand and the region as a whole. Despite this matrix of variable forest conditions, lidar data were able to account for a significant amount of variation in measured LAI for both individual study areas and when generalized to a region. SPOT data, when added to lidar-derived models, only slightly increased overall performance, yet contributed no additional predictive value for others aside from slightly reducing residual errors. Of notable importance, however, were the robust estimates of LAI quantities for the COMBINED dataset, which incorporated lidar data with slightly different acquisition parameters. This study has demonstrated the potential for lidar datasets with similar acquisition parameters to be merged for region-wide estimates of LAI. This finding is significant because it indicates that lidar data sharing through regional collaboration among agencies, corporations, and research institutions may facilitate the development of improved LAI datasets for specific ecosystems and regions.

LAI modeling within a multiple regression framework resulted in robust estimates across a range of physiographic conditions present in north Idaho, though generalized errors of corrected LAI were substantially larger than effective LAI. Because the RMSE for corrected LAI was 1.8 and 1.3 (i.e. 35% and 52% of the mean lidar-estimated LAI values) for the SJW and NPR, respectively, the application of a global regression model to map corrected LAI would result in area-wide estimates that could still introduce substantial error into subsequent ecological and/or biophysical modeling scenarios. As a result, future LAI mapping efforts that incorporate the fundamental contribution of species- and canopy architecture-specific clumping indices need to be taken into account to generate spatially-distributed estimates for this region and beyond (Chen et al., 2005a).

Acknowledgements

References

Allen, D.M. (1971). The prediction sum of squares as a criterion for selecting predictor variables. Univ. of Ky. Dept. of Statistics, Tech. Report 25.

Band, L., Peterson, D., Running, S. W., Coughlan, J., Lammers, R., Dungan, J., et al. (1991). Forest ecosystem processes at the watershed scale: Basis for distributed simulation. *Ecological Modeling*, 56, 171–196.

Baret, F., Hagolle, O., Geiger, B., Bicheron, P., Miras, B., Huc, M., et al. (2007). LAI, fAPAR and fCover CYCLOPES global products derived from VEGETATION: Part 1: Principles of the algorithm. *Remote Sensing of Environment*, 110, 275–286.

Birth, G. S., & McVey, G. (1968). Measuring the color of growing turf with a reflectance spectroradiometer. *Agronomy Journal*, 60, 640–643.

Blackburn, G. A. (2002). Remote sensing of forest pigments using airborne imaging spectrometer and LIDAR imagery. *Remote Sensing of Environment*, 82, 311–321.

Brown, L., Chen, J. M., Leblanc, S. G., & Chilar, J. (2000). A shortwave infrared modification to the simple ratio for LAI retrieval in boreal forests. An image and model analysis. *Remote Sensing of Environment*, 71, 16–25.

Chen, J. M., & Chilar, J. (1995). Quantifying the effect of canopy architecture on optical measurements of leaf area index using two gap size analysis methods. *IEEE Transactions on Geoscience and Remote Sensing*, 33, 216–777.

Chen, J. M., & Cihlar, J. (1996). Retrieving leaf area index of boreal conifer forests using Landsat TM images. *Remote Sensing of Environment*, 55, 153–162.

Chen, J. M., Govind, A., Sonnentag, O., Zhang, Y., Barr, A., & Amiro, B. (2006). Leaf area index measurements at Fluxnet-Canada forest sites. *Agricultural and Forest Meteorology*, 140, 257–268.

Chen, J. M., Menges, C. H., & Leblanc, S. G. (2005a). Global mapping of foliage clumping index using multi-angular satellite data. *Remote Sensing of Environment*, 97, 447–457.

Chen, X. X., Vierling, L., Deering, D., & Conley, A. (2005b). Monitoring boreal forest leaf area index across a Siberian burn chronosequence: A MODIS validation study. *International Journal of Remote Sensing*, 26, 5433–5451.

Chen, J. M., Pavlic, G., Brown, L., Cihlar, J., Leblanc, S. G., White, H. P., Hall, R. J., Peddle, D. R., King, D. J., Trofymow, J. A., Swift, E., Van der Sanden, J., & Pellikka, P. K. E. (2002). Derivation and validation of Canada-wide coarse-resolution leaf area index maps using high-resolution satellite imagery and ground measurements. *Remote Sensing of Environment*, 80, 165–184.

Chen, J. M., Rich, P. M., Gower, T. S., Norman, J. M., & Plummer, S. (1997). Leaf area index of boreal forests: Theory, techniques and measurements. *Journal of Geophysical Research*, 102, 429–443.

Chen, X. X., Vierling, L., Rowell, E., & DeFelice, T. (2004). Using lidar and effective LAI data to evaluate IKONOS and Landsat 7 ETM+ vegetation cover estimates in a ponderosa pine forest. *Remote Sensing of Environment*, 91, 14–26.

Clawges, R., Vierling, L. A., Calhoon, M., & Toomey, M. P. (2007). Use of a ground-based scanning lidar for estimation of biophysical properties of western larch (*Larix occidentalis*). *International Journal of Remote Sensing*, 28(19), 4331–4344.

Cohen, W. B., Maiersperger, T. K., Gower, S. T., & Turner, D. P. (2003). An improved strategy for regression of biophysical variables and Landsat ETM+ data. *Remote Sensing of Environment*, 84, 561–571.

Coops, N. C., Hilker, T., Wulder, M. A., St-Onge, B., Newnham, G., Siggins, A., et al. (2007). Estimating canopy structure of Douglas-fir forest stands from discrete-return lidar. *Trees - Structure and Function*, 21, 295–310.

Coops, N. C., Smith, M. L., Jacobsen, K. L., Martin, M., & Ollinger, S. (2004). Estimation of plant and leaf area index using three techniques in a mature native eucalypt canopy. *Austral Ecology*, 29, 332–341.

Cosmopoulos, P., & King, D. J. (2004). Temporal analysis of forest structural condition at an acid mine site using multispectral digital camera imagery. *International Journal of Remote Sensing*, 25, 2259–2275.

Curran, P. J., Dungan, J. L., & Gholz, H. L. (1992). Seasonal LAI in slash pine estimated with Landsat TM. *Remote Sensing of Environment*, 39, 3–13.

Curran, P. J., & Hay, A. (1986). The importance of measurement error for certain procedures in remote sensing at optical wavelengths. *Photogrammetric Engineering and Remote Sensing*, 52, 229–241.

Danson, F. M., Hetherington, D., Morsdorf, F., Koetz, B., & Allgower, B. (2007). Forest canopy gap fraction from terrestrial laser scanning. *Geoscience and Remote Sensing Letters, IEEE*, 4, 157–160.

Duursma, R. A., Marshall, J. D., & Robinson, A. P. (2003). Leaf area index inferred from solar beam transmission in mixed conifer forests on complex terrain. *Agricultural and Forest Meteorology*, 118, 221–236.

Ellsworth, D. S., & Reich, P. B. (1993). Canopy structure and vertical patterns of photosynthesis and related leaf traits in a deciduous forest. *Oecologia*, 96(2), 169–178.

Evans, J. S., & Hudak, A. T. (2007). A multiscale curvature algorithm for classifying discrete return lidar in forested environments. *IEEE Transactions on Geoscience and Remote Sensing*, 45, 1029–1038.

Falkowski, M. J., Gessler, P. E., Morgan, P., Hudak, A. T., & Smith, A. M. S. (2005). Characterizing and mapping forest fire fuels using ASTER imagery and gradient modeling. *Forest Ecology and Management*, 217, 129–146.

Fernandes, R., & Leblanc, S. G. (2005). Parametric (modified least squares) and non-parametric (Theil–Sen) linear regressions for predicting biophysical parameters in the presence of measurement errors. *Remote Sensing of Environment*, 95, 303–316.

Fournier, R. A., Mailly, D., Walter, J. -M. N., & Soudani, K. (2003). Indirect measurement of forest canopy structure from in situ optical sensors. In M. Wulder & S.E. Franklin (Eds.), *Remote Sensing of Forest Environments: Concepts and Case Studies* (pp. 77–113). Norwell, Massachusetts, USA: Kluwer Academic Press.

Frazer, G. W., Trofymow, J. A., & Lertzman, K. P. (2000). Canopy openness and leaf area in chronosequences of coastal temperate rainforests. *Canadian Journal of Forest Research*, 30, 239–256.

Friedl, M. A., Michaelson, J., Davis, F. W., Walker, H., & Schimel, D. S. (1994). Estimating grassland biomass and leaf area index using ground and satellite data. *International Journal of Remote Sensing*, 15, 1401–1420.

Gitelson, A. A., Vina, A., Arkebauer, T. J., Rundquist, D. C., Keydan, G., & Leavitt, B. (2004). Remote estimation of leaf area index and green leaf biomass in maize canopies. *Journal of Plant Physiology*, 165–173.

Gower, S. T., Kucharik, C. J., & Norman, J. M. (1999). Direct and indirect estimation of Leaf Area Index, fAPAR, and net primary production of terrestrial ecosystems. *Remote Sensing of Environment*, 70, 29–51.

Grier, C. G., & Running, S. W. (1977). Leaf area of mature northwestern coniferous forests: relation to site water balance. *Ecology*, 58, 893–899.

Hall, R. J., Davidson, D. P., & Peddle, D. R. (2003). Ground and remote estimation of leaf area in Rocky Mountain forest stands, Kananaskis, Alberta. *Canadian Journal of Remote Sensing*, 29, 411–427.

Hopkinson, C., & Chasmer, L. E. (2007). Modelling canopy gap fraction from lidar intensity. *ISPRS Workshop on Laser Scanning 2007 and SilviLaser 2007* Finland: Espoo.

Hudak, A. T., Crookston, N. L., Evans, J. S., Falkowski, M. J., Smith, A. M. S., Gessler, P. E., et al. (2006). Regression modeling and mapping of coniferous forest basal area and tree density from discrete-return lidar and multispectral satellite data. *Canadian Journal of Remote Sensing*, 32, 126–138.

Hudak, A. T., Lefsky, M. A., Cohen, W. B., & Berterretche, M. (2002). Integration of lidar and Landsat ETM plus data for estimating and mapping forest canopy height. *Remote Sensing of Environment*, 82, 397–416.

Huete, A. R., Liu, H. Q., Batchily, K., & van Leeuwen, W. (1997). A comparison of vegetation indices over a global set of TM images for EOS-MODIS. *Remote Sensing of Environment*, 59.

Jacquemoud, S., Baret, F., Andrieu, B., Danson, F. M., & Jaggard, K. (1995). Extraction of vegetation biophysical parameters by inversion of the PROSPECT+SAIL models on sugar beet canopy reflectance data. Application to TM and AVIRIS sensors. *Remote Sensing of Environment*, 52, 163–172.

Jensen, J. L. R., Humes, K. S., Conner, T., Williams, C. J., & DeGroot, J. (2006). Estimation of biophysical characteristics for highly variable mixed-conifer stands using small-footprint lidar. *Canadian Journal of Forest Research*, 36, 1129–1138.

Koetz, B., Morsdorf, F., Ranson, K. J., Itten, K., & Allgower, B. (2006). Inversion of a lidar waveform model for forest biophysical parameter estimation. *IEEE Transactions on Geoscience and Remote Sensing*, 3, 49–53.

Law, B. E., Cescatti, A., & Baldocchi, D. D. (2001a). Leaf area distribution and radiative transfer in open-canopy forests: Implications for mass and energy exchange. *Tree Physiology*, 21, 777–787.

Law, B. E., Van Tuyl, S., Cescatti, A., & Baldocchi, D. D. (2001b). Estimation of leaf area index in open-canopy ponderosa pine forests at different successional stages and management regimes in Oregon. *Agricultural and Forest Meteorology*, 108, 1–14.

Lefsky, M. A., Cohen, W. B., Acker, S. A., Parker, G. G., Spies, T. A., & Harding, D. (1999). Lidar remote sensing of the canopy structure and biophysical properties of Douglas-Fir Western Hemlock Forests. *Remote Sensing of Environment*, 70, 339–361.

Lefsky, M. A., Hudak, A. T., Cohen, W. B., & Acker, S. A. (2005a). Geographic variability in lidar predictions of forest stand structure in the Pacific Northwest. *Remote Sensing of Environment*, 95, 532–548.

Lefsky, M. A., Turner, D. P., Guzy, M., & Cohen, W. B. (2005b). Combining lidar estimates of aboveground biomass and Landsat estimates of stand age for spatially extensive validation of modeled forest productivity. *Remote Sensing of Environment*, 95, 549–558.

Lovell, J. L., Jupp, D. L. B., Culvenor, D. S., & Coops, N. C. (2003). Using airborne and ground-based ranging lidar to measure canopy structure in Australian forests. *Canadian Journal of Remote Sensing*, 29, 607–622.

Lymburner, L., Beggs, P. J., & Jacobson, C. R. (2000). Estimation of canopy-average surface-specific leaf area using Landsat TM data. *Photogrammetric Engineering and Remote Sensing*, 66, 183–191.

Maclean, G. A., & Krabill, W. B. (1986). Gross-merchantable timber volume estimation using an airborne LIDAR system. *Canadian Journal of Remote Sensing*, 12, 7–18.

Magnussen, S., & Boudewyn, P. (1998). Derivations of stand heights from airborne laser scanner data with canopy-based quantile estimators. *Canadian Journal of Forest Research*, 28, 1016–1031.

McCombs, J. W., Roberts, S. D., & Evans, D. L. (2003). Influence of fusing lidar and multispectral imagery on remotely sensed estimates of stand density and mean tree height in a managed loblolly pine plantation. *Forest Science*, 49, 457–466.

McMurtrie, R. E., & Landsberg, J. J. (1992). Using a simulation model to evaluate the effects of water and nutrients on the growth and carbon partitioning of Pinus radiata. *Forest Ecology and Management*, 61, 91–108.

Means, J. E., Acker, S. A., Fitt, B. J., Renslow, M., Emerson, L., & Hendrix, C. J. (2000). Predicting forest stand characteristics with airborne scanning lidar. *Photogrammetric Engineering and Remote Sensing*, 66, 1367–1371.

Morsdorf, F., Kotz, B., Meier, E., Itten, K. I., & Allgower, B. (2006). Estimation of LAI and fractional cover from small footprint airborne laser scanning data based on gap fraction. *Remote Sensing of Environment*, 104, 50–61.

Naesset, E., & Bjerknes, K. -O. (2001). Estimating tree heights and number of stems in young forest stands using airborne laser scanner data. *Remote Sensing of Environment*, 78, 328–340.

Nelson, R., Krabill, W., & Tonelli, J. (1988). Estimating forest biomass and volume using airborne laser data. *Remote Sensing of Environment*, 24, 247–267.

Nemani, R., Pierce, L., Running, S., & Band, L. (1993). Forest ecosystem processes at the watershed scale: Sensitivity to remotely sensed leaf area index estimates. *International Journal of Remote Sensing*, 14, 2519–2534.

Neter, J., Wasserman, W., & Kutner, M. H. (1985). *Applied Linear Statistical Models* (pp. 1152). Homewood, IL: Irwin.

Olthof, I., & King, D. J. (2000). Development of a forest health index using multispectral airborne digital camera imagery. *Canadian Journal of Remote Sensing*, 26, 166–175.

Pocewicz, A. L., Gessler, P., & Robinson, A. P. (2004). The relationship between effective plant area index and Landsat spectral response across elevation, solar insolation, and spatial scales in a northern Idaho forest. *Canadian Journal of Forest Research*, 34, 465–480.

Pocewicz, A., Vierling, L. A., Lentile, L. B., & Smith, R. (2007). View angle effects on relationships between MISR vegetation indices and leaf area index in a recently burned ponderosa pine forest. *Remote Sensing of Environment*, 107, 322–333.

Popescu, S. C., & Wynne, R. H. (2004). Seeing the trees in the forest: Using lidar and multispectral data fusion with local filtering and variable window size for estimating tree height. *Photogrammetric Engineering and Remote Sensing*, 70, 589–604.

Popescu, S. C., Wynne, R. H., & Nelson, R. F. (2003). Measuring individual tree crown diameter with lidar and assessing its influence on estimating forest volume and biomass. *Canadian Journal of Remote Sensing*, 29, 564–577.

Popescu, S. C., Wynne, R. H., & Scrivani, J. A. (2004). Fusion of small-footprint lidar and multispectral data to estimate plot-level volume and biomass in deciduous and pine forests in Virginia, USA. *Forest Science*, 50, 551–565.

Riano, D., Valladares, F., Condes, S., & Chuvieco, E. (2004). Estimation of leaf area index and covered ground from airborne laser scanner (Lidar) in two contrasting forests. *Agricultural and Forest Meteorology*, 124, 269–275.

Rich, P. M., Clark, D. B., Clak, D. A., & Oberbauer, S. F. (1993). Long-term study of solar radiation regimes in a tropical wet forest using quantum sensors and hemispherical photography. *Agricultural and Forest Meteorology*, 65, 107–127.

Roberts, D. A., Ustin, S. L., Ogunjemiyo, S., Greenberg, J., Dobrowski, S. Z., Chen, J. Q., & Hinckley, T. M. (2004). Spectral and structural measures of northwest forest vegetation at leaf to landscape scales. *Ecosystems*, 7, 545–562.

Rouse, J. W., Haas, R. H., Deering, D. W., Schell, J. A., & Harlan, J. C. (1974). Monitoring vegetation systems in the Great Plains with ERTS. *Proceedings, 3rd Earth Resource Technology Satellite (ERTS) Symposium* (pp. 48–62).

Running, S. W., & Coughlan, J. C. (1988). A general model of forest ecosystem processes for regional applications I. Hydrologic balance, canopy gas exchange and primary production processes. *Ecological Modeling*, 42, 125–154.

Running, S. W., Peterson, D. L., Spanner, M. A., & Teuber, K. B. (1986). Remote sensing of coniferous Forest Leaf Area. *Ecology*, 67, 273–276.

Schimel, D., Kittel, T., Running, S., Monson, R., Turnipseed, A., & Anderson, D. (2002). Carbon sequestration studies in Western U.S. mountains. *EOS Transactions* (pp. 445–449). : American Geophysical Union.

Stenberg, P., Rautiainen, M., Manninen, T., Voipio, P., & Smolander, H. (2004). Reduced simple ratio better than NDVI for estimating LAI in Finnish pine and spruce stands. *Silva Fennica*, 38, 3–14.

Suguira, N. (1978). Further analysis of the data by Akaike's information criterion and the finite corrections. *Communication in Statistics, A*, 7, 13–26.

Tucker, C. J. (1979). Red and photographic infrared linear combinations for monitoring vegetation. *Remote Sensing of Environment*, 8, 127–150.

Turner, D. P., Cohen, W. B., Kennedy, R. E., Fassnacht, K. S., & Briggs, J. M. (1999). Relationships between leaf area index and Landsat spectral vegetation indices across three temperate zone sites. *Remote Sensing of Environment*, 70, 52–68.

Vierling, L. A., & Wessman, C. A. (2000). Photosynthetically active radiation heterogeneity within a monodominant Congolese rain forest canopy. *Agricultural and Forest Meteorology*, 103, 265–278.

Walthall, C., Dulaney, W., Anderson, M., Norman, J., Fang, H., & Liang, S. (2004). A comparison of empirical and neural network approaches for estimating corn and soybean leaf area index from Landsat ETM+ imagery. *Remote Sensing of Environment*, 92, 465–474.

Welles, J. M., & Norman, J. M. (1991). Instrument for indirect measurement of canopy architecture. *Agronomy Journal*, 83, 818–825.

White, J. D., Running, S. W., Nemani, R., Keane, R. E., & Ryan, K. C. (1997). Measurement and remote sensing of LAI in Rocky Mountain montane ecosystems. *Canadian Journal of Forest Research*, 27, 1714–1727.

Wulder, M. A., Han, T., White, J. C., Sweda, T., & Tsuzuki, H. (2007). Integrating profiling LIDAR with Landsat data for regional boreal forest canopy attribute estimation and change characterization. *Remote Sensing of Environment*, 110, 123–137.

Wulder, M. A., LeDrew, E. F., Franklin, S. E., & Lavigne, M. B. (1998). Aerial image texture information in the estimation of Northern Deciduous and Mixed Wood Forest Leaf Area Index (LAI). *Remote Sensing of Environment*, 64, 64–76.

Wulder, M. A., & Seemann, D. (2003). Forest inventory height update through the integration of lidar data with segmented Landsat imagery. *Canadian Journal of Remote Sensing*, 29, 536–543.

Yang, W., Tan, B., Huang, D., Rautiainen, M., Shabanov, N. V., Wang, Y., et al. (2006). MODIS leaf area index products: From validation to algorithm improvement. *IEEE Transactions on Geoscience and Remote Sensing*, 44, 1885–1898.